Available online at www.sciencedirect.com
ScienceDirect
International Journal of Solids and Structures 44 (2007) 8074–8085
INTERNATIONAL JOURNAL OF SOLIDS AND STRUCTURES
www.elsevier.com/locate/ijsolstr

Buckling of a pre-compressed or pre-stretched membrane in shear flow

H. Luo [a], C. Pozrikidis [b,*]

[a] Department of Mechanical Engineering, Vanderbilt University, VU Station B 351592, 2301 Vanderbilt Pl, Nashville, TN 37235-1592, USA
[b] Department of Mechanical and Aerospace Engineering, University of California, San Diego, La Jolla, CA 92093-0411, USA

Received 14 November 2006; received in revised form 2 May 2007
Available online 10 June 2007

Abstract

Membranes enclosing capsules and biological cells undergo periodic compression and stretching due to an imparted hydrodynamic traction as they rotate in a shear flow. Compression may cause transient or permanent buckling manifested by the onset of wrinkled shapes. To study the effect of pre-compression and pre-stretching on the critical conditions for buckling, the response of an elastic circular plate flush mounted on a plane wall and deforming under the action of a uniform tangential load due to an over-passing simple shear flow is considered. Working under the auspices of the theory of elastic instability of plates governed by the linear von Kármán equation, an eigenvalue problem is formulated resulting in a fourth-order partial differential equation with position-dependent coefficients parametrized by the Poisson ratio. Solutions are computed by applying Fourier series expansions to derive an infinite system of coupled ordinary differential equations, and then implementing orthogonal collocation. The solution space is illustrated, critical values for buckling are identified, the associated eigenfunctions representing possible modes of deformation are displayed, and the effect of the Poisson ratio is discussed.

Keywords: Membrane wrinkling; Capsules; Elastic instability; Plate buckling; Shear flow

1. Introduction

Recent experiments have shown that a spherical capsule enclosing a liquid and bounded by an elastic membrane may develop corrugations described as wrinkles when subjected to a simple shear flow (Walter et al., 2001). The most probable physical reason is that the membrane is locally subjected to a compressive load that causes buckling above a certain threshold. The onset and severity of buckling are affected by the membrane thickness and material constitution determining the membrane flexural stiffness, as well as by the duration of the compressive load on a rotating membrane patch that carries the hydrodynamic load. Lac and Barthés-Biesel (2005)

* Corresponding author. Tel.: +1 858 534 6530; fax: +1 858 534 7078.
E-mail address: cpozrikidis@ucsd.edu (C. Pozrikidis).

0020-7683/$ - see front matter © 2007 Elsevier Ltd. All rights reserved.
doi:10.1016/j.ijsolstr.2007.05.027

demonstrated that buckling is suppressed when the membrane is sufficiently pre-stretched, so that the compressive load is either diminished or altogether disappears.

To study the suppression mechanism, we consider the buckling of a pre-compressed or pre-stretched circular membrane patch flush mounted on a plane wall. In our terminology, "membrane" refers to a biological object rather than a thin shell with infinitesimal bending stiffness, as it is traditionally implied in mechanics. The circular patch represents a small section of a stationary or rotating capsule membrane, serving as a local model of the membrane. A simple shear flow occurs on both sides of the patch emulating the flow in the capsule exterior and interior.

The hydrodynamic shear stress imparts to the membrane a tangential load that amounts to a uniform body force. Elementary mechanics indicates that the upstream part of the membrane is stretched, while the downstream part is compressed. Compression raises the possibility of buckling when the uniform load exceeds a critical threshold representing a bifurcation point in the solution space. The computation of these bifurcation points and associated eigenfunctions is the main objective of our work. The analysis and results extend the recent work of Luo and Pozrikidis (2006) on the buckling of elastic plates with arbitrary shapes flush mounted on a rigid wall in the absence of pre-stress.

In Section 2, the physical problem is described and an eigenvalue problem is formulated based on the linear von Kármán equation for elastic plates. In Section 3, a numerical method based on a Fourier series expansions is developed. Numerical results are presented in Sections 4 and 5, and the new findings are summarized in Section 6.

2. Theoretical model

We consider a uniformly pre-compressed or pre-stretched elastic membrane flush mounted on a rigid wall with its edge clamped around the rim, as illustrated in Fig. 1. The upper and lower surfaces of the membrane are exposed to an over-passing shear flow along the x axis with velocity $u_x = G_1 z$ above the membrane and $u_x = G_2 z$ below the membrane, where G_1 and G_2 are constant shear rates, and the z axis is normal to the wall. The shear flow imparts to the upper and lower surfaces of the membrane a uniform hydrodynamic shear stress, $\tau_1 = \mu_1 G_1$ and $\tau_2 = \mu_2 G_2$, where μ_1 and μ_2 are the fluid viscosities.

Working under the auspices of thin-shell theory, we smear the tangential membrane load due to the hydrodynamic shear stress from the membrane surfaces into the membrane cross-section to obtain an in-plane body force with components

$$b_x = \frac{\Delta\tau}{h}, \quad b_y = 0, \tag{1}$$

where

$$\Delta\tau \equiv \tau_1 - \tau_2 = \mu_1 G_1 - \mu_2 G_2 \tag{2}$$

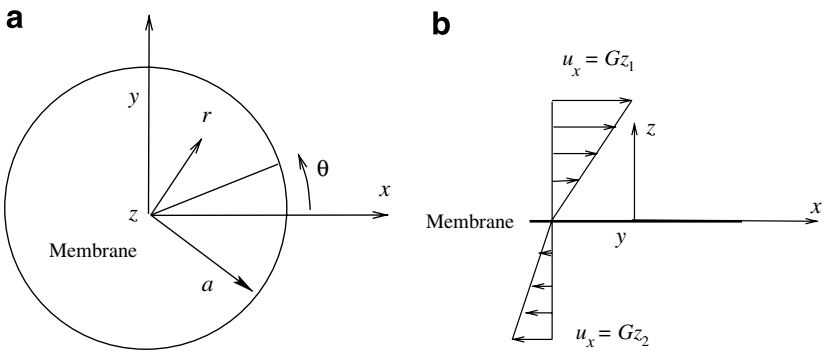

Fig. 1. Shear flow past a circular membrane patch modeled as an elastic plate flush mounted on a plane wall. A shear flow parallel to the membrane occurs on either side. (a) Top view, and (b) side view.

is the tangential hydrodynamic load, and h is the membrane thickness.

We assume that the in-plane stresses developing due to the in-plane deformation of the membrane in the absence of buckling, σ_{ij}, are related to the in-plane strains, ϵ_{ij}, by the linear constitutive equation

$$\begin{bmatrix} \sigma_{xx} \\ \sigma_{yy} \\ \sigma_{xy} \end{bmatrix} = \frac{E}{1-\nu^2} \begin{bmatrix} 1 & \nu & 0 \\ \nu & 1 & 0 \\ 0 & 0 & 1-\nu \end{bmatrix} \cdot \begin{bmatrix} \epsilon_{xx} \\ \epsilon_{yy} \\ \epsilon_{xy} \end{bmatrix}, \tag{3}$$

where

$$\epsilon_{kl} = \frac{1}{2}\left(\frac{\partial v_k}{\partial x_l} + \frac{\partial v_l}{\partial x_k}\right), \tag{4}$$

(v_x, v_y) is the tangential displacement of membrane point particles in the xy plane, E is the membrane modulus of elasticity, and ν is the Poisson ratio. The upper limit, $\nu = 0.5$, corresponds to an incompressible material. Although the Poisson ratio is positive for the vast majority of materials encountered in practice, zero or slightly negative values have been reported for wrinkled membranes (Pieper et al., 1988). Physically, smoothing of the wrinkles under uniaxial extension leads to expansion in the lateral direction associated with a negative Poisson ratio (Boal et al., 1993; Schmid-Schoenbein et al., 1995). Force equilibrium requires the differential balances

$$\frac{\partial \sigma_{xx}}{\partial x} + \frac{\partial \sigma_{yx}}{\partial y} + b_x = 0, \quad \frac{\partial \sigma_{xy}}{\partial x} + \frac{\partial \sigma_{yy}}{\partial y} + b_y = 0, \tag{5}$$

subject to the boundary conditions $v_x = 0$ and $v_y = 0$ around the clamped rim. In the case of a circular membrane of radius a, elementary analysis shows that

$$v_x = \frac{\Delta\tau}{Eh}\frac{1-\nu^2}{3-\nu}(a^2 - x^2 - y^2) + \frac{1-\nu}{E}\sigma_0 x, \quad v_y = \frac{1-\nu}{E}\sigma_0 y, \tag{6}$$

and

$$\sigma_{xx} = -\frac{2}{3-\nu}\frac{\Delta\tau}{h}x + \sigma_0, \quad \sigma_{xy} = -\frac{1-\nu}{3-\nu}\frac{\Delta\tau}{h}y, \quad \sigma_{yy} = -\frac{2\nu}{3-\nu}\frac{\Delta\tau}{h}x + \sigma_0, \tag{7}$$

where σ_0 is the positive or negative membrane pre-stress. In the absence of pre-stress, $\sigma_0 = 0$, the streamwise component of the in-plane normal stress, σ_{xx}, is positive (tensile) on the upstream half of the membrane, and negative (compressive) on the downstream half of the membrane. The transverse component of the normal stress, σ_{yy}, is also positive or negative depending on the sign of the Poisson ratio.

Compression raises the possibility of buckling when the pre-compression is sufficiently strong or the tangential hydrodynamic load exceeds a critical threshold. To compute the transverse deflection along the z axis upon inception of buckling, we work under the auspices of linear elastic instability of thin plates and shells, and derive the linear von Kármán equation for the deflection function $z = f(x, y)$,

$$\begin{aligned} \nabla^4 f \equiv \nabla^2\nabla^2 f &= \frac{\partial^4 f}{\partial x^4} + 2\frac{\partial^4 f}{\partial x^2 \partial y^2} + \frac{\partial^4 f}{\partial y^4} \\ &= \frac{h}{E_B}\left(\sigma_{xx}\frac{\partial^2 f}{\partial x^2} + 2\sigma_{xy}\frac{\partial^2 f}{\partial x \partial y} + \sigma_{yy}\frac{\partial^2 f}{\partial y^2} - b_x\frac{\partial f}{\partial x} - b_y\frac{\partial f}{\partial y}\right), \end{aligned} \tag{8}$$

where E_B is the membrane modulus of bending (e.g., Bloom and Coffin, 2001, p. 18, Timoshenko and Gere, 1961, p. 305); for an elastic plate, $E_B = Eh^3/[12(1-\nu^2)]$ (e.g., Fung, 1965, p. 461, Timoshenko and Gere, 1961, p. 335). The fourth-order differential Eq. (8) involves position-dependent coefficients multiplying the second derivatives on the right-hand side. Substituting in (8) expressions (7) for the in-plane stresses and expression (1) for the body force, we obtain

$$\nabla^4 f = -\frac{1}{a^3}\left[(\alpha x - \beta a)\frac{\partial^2 f}{\partial x^2} + \alpha(1-\nu)y\frac{\partial^2 f}{\partial x \partial y} + (\nu\alpha x - \beta a)\frac{\partial^2 f}{\partial y^2} + \alpha\frac{3-\nu}{2}\frac{\partial f}{\partial x}\right], \tag{9}$$

where

$$\alpha \equiv \frac{2\Delta\tau a^3}{E_B(3-\nu)}, \quad \beta = \frac{\sigma_0 h a^2}{E_B} \tag{10}$$

are two dimensionless parameters expressing the hydrodynamic load and pre-stress. In terms of the dimensionless parameters α and β, the in-plane tensions are given by

$$\begin{aligned} \sigma_{xx} &= \frac{E_B}{ha^2}\left(-\alpha\frac{x}{a}+\beta\right), \quad \sigma_{xy} = -\frac{E_B(1-\nu)}{2ha^2}\alpha\frac{y}{a}, \\ \sigma_{yy} &= \frac{E_B}{ha^2}\left(-\nu\alpha\frac{x}{a}+\beta\right). \end{aligned} \tag{11}$$

The streamwise tension, σ_{xx}, is positive over the whole area of the membrane as long as $\alpha < \beta$, whereas the transverse tension, σ_{yy}, is positive as long as $\alpha < \beta/\nu$. Since $\nu < 1$, we require positivity of σ_{xx} and obtain a conservative criterion for the onset of buckling.

The solution is to be found subject to the homogeneous Dirichlet and Neumann boundary conditions, $f = 0$ and $\partial f/\partial r = 0$ at $r = a$, where r is the distance from the origin. Eq. (9) admits the trivial solution, $f = 0$, for any values of α and β, and non-trivial eigensolutions at a sequence of discrete eigenvalues. The computation of these eigenvalues and corresponding eigenfunctions is the main objective of our work.

3. Fourier expansion

It is convenient to work in the plane polar coordinates defined in Fig. 1, and non-dimensionalize the position, radial distance, and membrane deflection by the patch radius, a. Dimensionless variables are indicated by a hat; for example, $\hat{r} = r/a$ and $\hat{f} = f/a$. An eigenfunction of (9) can be expanded in a Fourier series,

$$\hat{f}(\hat{r},\theta) = \frac{1}{2}p_0(\hat{r}) + \sum_{n=1}^{\infty}(p_n(\hat{r})\cos n\theta + q_n(\hat{r})\sin n\theta) = \sum_{n=-\infty}^{\infty} F_n(\hat{r})\exp(-\mathrm{i}n\theta), \tag{12}$$

where i is the imaginary unit, $p_n(\hat{r})$ and $q_n(\hat{r})$ are real dimensionless functions, and $F_n(\hat{r})$ is a complex dimensionless function. We have adopted Euler's formula for the complex exponential $\exp(-\mathrm{i}n\theta) = \cos(n\theta) - \mathrm{i}\sin(n\theta)$. The complex functions, $F_n(\hat{r})$, is defined such that

$$F_n(\hat{r}) \equiv \frac{1}{2}(p_n(\hat{r}) + \mathrm{i}q_n(\hat{r})) \tag{13}$$

for $n \geqslant 0$ and $F_n(\hat{r}) = F^*_{-n}(\hat{r})$, where an asterisk denotes the complex conjugate. To ensure that the deflected membrane shape is smooth at the origin, we require $F_n(0) = 0$ for $n \geqslant 1$. A straightforward computation yields the following expressions for the Laplacian and bi-Laplacian in plane polar coordinates:

$$\hat{\nabla}^2\hat{f} = \sum_{n=-\infty}^{\infty} Q_n(\hat{r})\exp(-\mathrm{i}n\theta), \quad \hat{\nabla}^4\hat{f} = \sum_{n=-\infty}^{\infty} \Omega_n(\hat{r})\exp(-\mathrm{i}n\theta), \tag{14}$$

where $\hat{\nabla}$ is the gradient with respect to $\hat{x} \equiv x/a$ and $\hat{y} \equiv y/a$,

$$Q_n \equiv F_n'' + \frac{F_n'}{\hat{r}} - n^2\frac{F_n}{\hat{r}^2}, \tag{15}$$

a prime denotes a derivative with respect to $\hat{r}$, and

$$\begin{aligned} \Omega_n(\hat{r}) &\equiv Q_n'' + \frac{Q_n'}{\hat{r}} - n^2\frac{Q_n}{\hat{r}^2} \\ &= F_n'''' + \frac{2}{\hat{r}}F_n''' - \frac{1+2n^2}{\hat{r}^2}F_n'' + \frac{1+2n^2}{\hat{r}^3}F_n' + n^2\frac{n^2-4}{\hat{r}^4}F_n. \end{aligned} \tag{16}$$

To also express the right-hand side of (9) in a Fourier series, we use the Cartesian to plane polar transformation rules:

$$
\begin{aligned}
\frac{\partial \hat{f}}{\partial \hat{x}} &= \cos\theta \frac{\partial \hat{f}}{\partial \hat{r}} - \frac{\sin\theta}{\hat{r}} \frac{\partial \hat{f}}{\partial \theta}, \\
\frac{\partial^2 \hat{f}}{\partial \hat{x}^2} &= \cos^2\theta \frac{\partial^2 \hat{f}}{\partial \hat{r}^2} - \frac{\sin 2\theta}{\hat{r}} \frac{\partial^2 \hat{f}}{\partial \hat{r}\partial\theta} + \frac{\sin^2\theta}{\hat{r}} \frac{\partial \hat{f}}{\partial \hat{r}} + \frac{\sin 2\theta}{\hat{r}^2} \frac{\partial \hat{f}}{\partial \theta} + \frac{\sin^2\theta}{\hat{r}^2} \frac{\partial^2 \hat{f}}{\partial \theta^2}, \\
\frac{\partial^2 \hat{f}}{\partial \hat{y}^2} &= \sin^2\theta \frac{\partial^2 \hat{f}}{\partial \hat{r}^2} + \frac{\sin 2\theta}{\hat{r}} \frac{\partial^2 \hat{f}}{\partial \hat{r}\partial\theta} + \frac{\cos^2\theta}{\hat{r}} \frac{\partial \hat{f}}{\partial \hat{r}} - \frac{\sin 2\theta}{\hat{r}^2} \frac{\partial \hat{f}}{\partial \theta} + \frac{\cos^2\theta}{\hat{r}^2} \frac{\partial^2 \hat{f}}{\partial \theta^2}, \\
\frac{\partial^2 \hat{f}}{\partial \hat{x}\partial \hat{y}} &= \frac{1}{2}\left(\sin 2\theta \frac{\partial^2 \hat{f}}{\partial \hat{r}^2} + 2\frac{\cos 2\theta}{\hat{r}} \frac{\partial^2 \hat{f}}{\partial \hat{r}\partial\theta} - \frac{\sin 2\theta}{\hat{r}} \frac{\partial \hat{f}}{\partial \hat{r}} - 2\frac{\cos 2\theta}{\hat{r}^2} \frac{\partial \hat{f}}{\partial \theta} - \frac{\sin 2\theta}{\hat{r}^2} \frac{\partial^2 \hat{f}}{\partial \theta^2} \right).
\end{aligned}
\tag{17}
$$

Using Euler's formula to express the cosines and sines in terms of the complex exponential and substituting the Fourier expansion, we find

$$
\begin{aligned}
\frac{\partial \hat{f}}{\partial \hat{x}} &= \frac{1}{2} \sum_{n=-\infty}^{\infty} \left[\left(F_n' + n\frac{F}{\hat{r}} \right) e^{i\theta} + \left(F_n' - n\frac{F}{\hat{r}} \right) e^{-i\theta} \right] \exp(-in\theta), \\
\frac{\partial^2 \hat{f}}{\partial \hat{x}^2} &= \frac{1}{2} \sum_{n=-\infty}^{\infty} \left[Q_n + R_n e^{2i\theta} + T_n e^{-2i\theta} \right] \exp(-in\theta), \\
\frac{\partial^2 \hat{f}}{\partial \hat{y}^2} &= \frac{1}{2} \sum_{n=-\infty}^{\infty} \left[Q_n - R_n e^{2i\theta} - T_n e^{-2i\theta} \right] \exp(-in\theta), \\
\frac{\partial^2 \hat{f}}{\partial \hat{x}\partial \hat{y}} &= -\frac{i}{2} \sum_{n=-\infty}^{\infty} \left[R_n e^{2i\theta} - T_n e^{-2i\theta} \right] \exp(-in\theta),
\end{aligned}
\tag{18}
$$

where

$$
\begin{aligned}
R_n &\equiv \frac{1}{2}\left(F_n'' + (2n-1)\frac{F_n'}{\hat{r}} + n(n-2)\frac{F_n}{\hat{r}^2} \right), \\
T_n &\equiv \frac{1}{2}\left(F_n'' - (2n+1)\frac{F_n'}{\hat{r}} + n(n+2)\frac{F_n}{\hat{r}^2} \right).
\end{aligned}
\tag{19}
$$

If the function F_n is real, $F_n = F_{-n}$, the functions R_n and T_n are related by $R_n = T_{-n}$.

Using these expressions, we find:

$$
\hat{\nabla}^4 \hat{f} = -\frac{1}{2} \sum_{n=-\infty}^{\infty} \left[\alpha \Psi_n e^{i\theta} - 2\beta Q_n + \alpha \Phi_n e^{-i\theta} \right] e^{-in\theta},
\tag{20}
$$

which can be restated as:

$$
\hat{\nabla}^4 \hat{f} = -\frac{1}{2} \sum_{n=-\infty}^{\infty} \left[\alpha \Psi_{n+1} - 2\beta Q_n + \alpha \Phi_{n-1} \right] e^{-in\theta},
\tag{21}
$$

where

$$
\begin{aligned}
\Psi_n &= \hat{r}F_n'' + \left[\frac{3+\nu}{2} + (1-\nu)n \right] F_n' + n\left(\frac{1+\nu}{2} - \nu n \right) \frac{F_n}{\hat{r}}, \\
\Phi_n &= \hat{r}F_n'' + \left[\frac{3+\nu}{2} - (1-\nu)n \right] F_n' - n\left(\frac{1+\nu}{2} + \nu n \right) \frac{F_n}{\hat{r}}.
\end{aligned}
\tag{22}
$$

Substituting (21) and (14) in (9) and equating corresponding Fourier coefficients, we derive an infinite tridiagonal system of ordinary differential equations,

$$
\Omega_n - \beta Q_n = -\frac{\alpha}{2}(\Psi_{n+1} + \Phi_{n-1}),
\tag{23}
$$

for $n = 0, \pm 1, \pm 2, \ldots$. Approximate eigenvalues are computed by truncating the system at a finite level, $n = \pm N$. In the case of eigensolutions with left-to-right symmetry with respect to the zx plane, the Fourier series involves only cosine terms, the component functions F_n are real, $F_n = F_{-n}$, and $\Psi_{-n} = \Phi_n$. The general system (23) then reduces to

$$\begin{aligned} \Omega_0 - \beta Q_0 &= -\alpha \Psi_1, \\ \Omega_n - \beta Q_n &= -\frac{\alpha}{2}(\Psi_{n+1} + \Phi_{n-1}), \end{aligned} \tag{24}$$

for $n = 1, 2, \ldots, N$. If the eigensolutions are antisymmetric with respect to the zx plane, the Fourier series involves only sine terms, the component functions F_n are imaginary, $F_n = -F_{-n}$, $\Psi_{-n} = -\Phi_n$, and $\Omega_0 - \beta Q_0 = 0$.

To satisfy the boundary conditions $F_n = F_n' = 0$ around the rim, we set

$$F_i = (1 - \hat{r})^2 H_i(\hat{r}), \tag{25}$$

and approximate the modulating functions $H_i(\hat{r})$ with Mth-degree polynomials in $\hat{r}$,

$$H_i(\hat{r}) = c_{i0} + c_{i1}\hat{r} + \cdots + c_{iM}\hat{r}^M, \tag{26}$$

where M is a specified polynomial order. Substituting (25) and (26) into the governing differential equations, computing the required derivatives analytically by differentiating the polynomials, and enforcing the resulting equations at the Chebyshev collocation points,

$$\hat{r}_j = \frac{t_j + 1}{2}, \qquad t_j = \cos\left[\left(j - \frac{1}{2}\right)\frac{\pi}{M+1}\right], \tag{27}$$

for $j = 1, 2, \ldots, M+1$, we obtain a generalized eigenvalue problem of the form

$$(\mathbf{A} - \beta \mathbf{B} - \alpha \mathbf{C}) \cdot \mathbf{c} = \mathbf{0}, \tag{28}$$

where the vector $\mathbf{c}$ contains the polynomial coefficients, c_{ij}. Specifically, the matrices $\mathbf{A}$ and $\mathbf{B}$ consist of $2N + 1$ diagonal blocks with dimensions $(M+1) \times (M+1)$, while the matrix $\mathbf{C}$ consists of $2N$ super-diagonal and sub-diagonal blocks with same dimensions.

For a specified dimensionless pre-stress, β, the numerical task is to compute as many eigenvalues α as possible, beginning with the smallest eigenvalue and moving upward. Physically, the highest eigenvalue is the minimum shear stress for buckling. Alternatively, for a specified dimensionless shear stress, α, the numerical task is to compute as many eigenvalues β as possible, beginning with the highest eigenvalue and moving downward. Physically, the highest eigenvalue represents the minimum pre-compression for buckling.

Since the matrices $\mathbf{A}$ and $\mathbf{B}$ arise from the discretization of the elliptic biharmonic operator, they are non-singular and well conditioned. By contrast, the matrix $\mathbf{C}$ is poorly conditioned. The computation of the eigenvalues was carried out using the Matlab `eig` function. Eigenvalues come in degenerate positive–negative pairs representing identical buckling states that arise when the shear flow is oriented toward the positive or negative direction of the x axis. The eigenfunctions are either symmetric or antisymmetric with respect to the zx plane, designated by S or A, respectively.

4. Buckling of a compressed membrane

In the absence of hydrodynamic load, $\alpha = 0$, the right-hand side of (23) is zero, the Fourier modes decouple, $\Omega_n = \beta\, Q_n$, for $n = 0, 1, 2, \ldots$, and the eigenvalue β represents the critical load for the buckling of a uniformly loaded circular membrane. The eigenvalues of axisymmetric buckling modes corresponding to $n = 0$ are the squares of the zeros of the Bessel function, $J_1(x)$ (e.g., Timoshenko and Gere, 1961, p. 390).

Due to the rotational symmetry, we may set $F_{-n} = F_n$ and expand the deflection, $\hat{f}(\hat{r}, \theta)$ in a cosine Fourier series. The eigenvalue problem is governed by the Bessel differential equation

$$R^2 \ddot{Q}_n(R) + R\dot{Q}_n(R) + (R^2 - n^2)Q_n(R) = 0, \tag{29}$$

where $R = \hat{r}\sqrt{-\beta}$, and a dot denotes a derivative with respect to R. To ensure regularity at the origin, we set

$$Q_n(R) = AJ_n(R), \tag{30}$$

where A is an arbitrary constant and J_n is a Bessel function. Using (15), we obtain a non-dimensional inhomogeneous equation for the shape function,

$$\ddot{F}_n + \frac{\dot{F}_n}{R} - n^2\frac{F_n}{R^2} + \frac{A}{\beta}J_n(R) = 0. \tag{31}$$

A solution satisfying $F_n = 0$ at $\hat{r} = 1$ corresponding to $R = \sqrt{-\beta}$, is

$$F_n(R) = B\left(J_n(R) - \frac{J_n(\sqrt{-\beta})}{(-\beta)^{n/2}}R^n\right), \tag{32}$$

where $B = A/\beta$. To also satisfy the boundary condition $\mathrm{d}F_n/\mathrm{d}\hat{r} = 0$ at $\hat{r} = 1$, we require $\beta = \beta_i = -z_i^2$, where z_i is a zero of the function

$$H(x) = J_n'(x) - n\frac{J_n(x)}{x} = J_{n+1}(x). \tag{33}$$

Thus, z_i is a zero of the Bessel function $J_{n+1}(z)$, which is consistent with the well-known results for $n = 0$. The deflected membrane shape is described by the equation:

$$\hat{f}(\hat{r},\theta) = C(J_n(z_i\hat{r}) - J_n(z_i)\hat{r}^n)\cos n\theta, \tag{34}$$

where C is an arbitrary constant. These results are independent of the Poisson ratio.

These analytical predictions are in excellent agreement with the results of our numerical computations listed in Table 1. The relative error is less than 10^{-5} for all modes considered. The computed buckled shapes for the first axisymmetric mode ($n = 0$) and buckling states $i = 1, 2$, and for the three non-axisymmetric modes ($n = 1, 2, 3$), and buckling state $i = 1$, are shown in Fig. 2.

Our analysis in the absence of shear flow complements the recent work of Wang (2005) on the buckling of a radially compressed circular plate resting on a Winkler foundation. As the elastic modulus of the foundation tends to zero, Wang (2005) found that the critical load tends to the limit identified in our analysis for the first non-axisymmetric mode.

5. Buckling in shear flow

Fig. 3 describes the structure of the solution space for the first symmetric mode (broken lines) and first antisymmetric mode (solid lines), in the β–α plane. The graphs illustrate the critical hydrodynamic load, α, for a certain pre-compression or pre-stretching, β, where the membrane first buckles. Alternatively, the graphs illustrate the pre-stress necessary to suppress buckling due to a certain hydrodynamic load.

The first symmetric solution branch in Fig. 3(a) originates from the critical point $\beta = -14.6820$, $\alpha = 0$, where the membrane buckles under a radially compressive pre-stress in the absence of a hydrodynamic load. The corresponding eigenmode describing an axisymmetric shape is shown in Fig. 2(a). By symmetry, this and all other branches cross the β axis at a right angle. Buckling does not occur for combinations (β, α) that lie underneath the first symmetric solution branch. The criterion of positive in-plane normal stresses discussed in Section 2 predicts stable shapes for (β, α) pairs that lie below the curve $\alpha = \beta$ drawn with the dotted line

Table 1
Buckling of a radially compressed circular membrane in the absence of hydrodynamic load

i	$n = 0$	$n = 1$	$n = 2$	$n = 3$	$n = 4$
1	−14.6820	−26.3746	−40.7065	−57.5829	−76.9389
2	−49.2185	−70.8500	−95.2776	−122.4278	−152.2412
3	−103.4995	−135.0207	−169.3955	−206.5698	−246.4955
4	−177.5208	−218.9202	−263.2033	−310.3223	−360.2455

The table gives the buckling thresholds β_i for the first few Fourier modes (n) and buckling states (i), computed with numerical truncation level $N = 20$. The $n = 0$ solutions yield axisymmetric shapes. The thresholds are independent of the Poisson ratio.

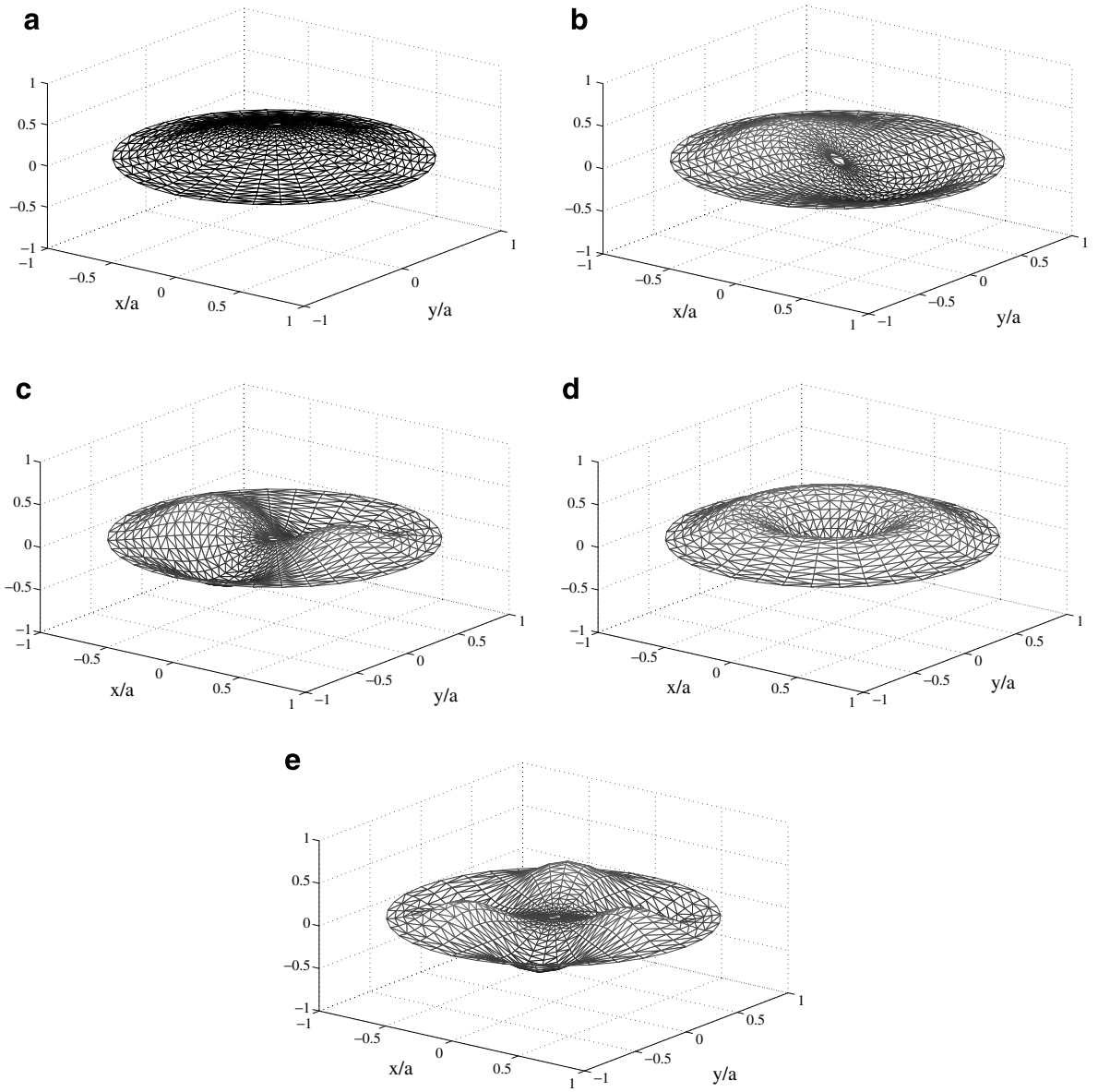

Fig. 2. Buckling of a radially compressed circular plate in the absence of hydrodynamic load. The graphs display the most dangerous buckling modes for (a) $\beta = -14.6820$ ($n = 0$, $i = 1$), (b) -26.3746 ($n = 1$, $i = 1$), (c) -40.7065 ($n = 2$, $i = 1$), (d) -49.2185 ($n = 0$, $i = 2$), and (e) -57.5829 ($n = 3$, $i = 1$).

in Fig. 3(a), which is seen to be highly conservative. Physically, the flat membrane tolerates compression over a portion of its surface without buckling, and the margin of tolerance increases when the membrane is pre-stretched.

As the value of β increases along the symmetric solution branch, the buckled shapes becomes increasingly non-axisymmetric and the critical value of α increases in a monotonic fashion. The trend continues as β becomes zero and then positive, where pre-compression transforms into pre-stretching. The critical value for an unstressed membrane, $\alpha = 72.71$ for $\beta = 0$, was identified previously by Luo and Pozrikidis (2006) by analytical methods and confirmed by finite element calculations. Buckled shapes for pre-compressed and a pre-stretched membrane, $\beta = -10$ and 10, are shown in Fig. 4(a and b). In agreement with intuition, the

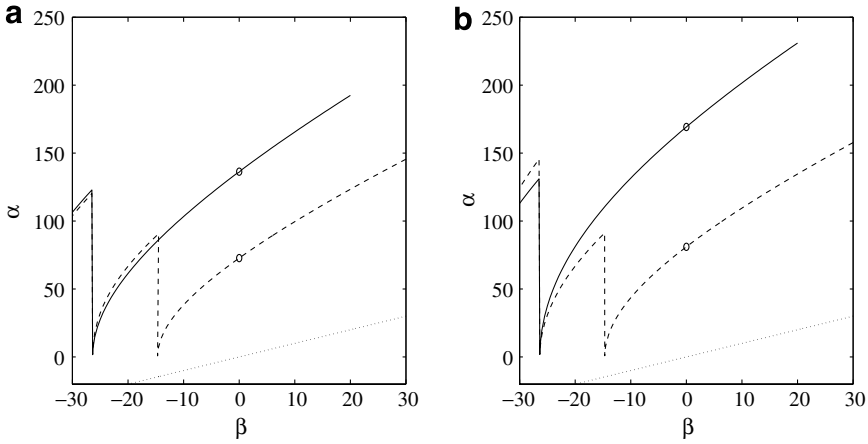

Fig. 3. Buckling of a radially compressed circular in the presence of hydrodynamic load. Solution branches of the lowest symmetric mode (broken line), and antisymmetric mode (solid line), for (a) $\nu = 0.45$, and (b) $\nu = 0.10$. The circles mark the critical conditions in the absence of pre-stress. The dotted line represents the conservative prediction, $\alpha = \beta$.

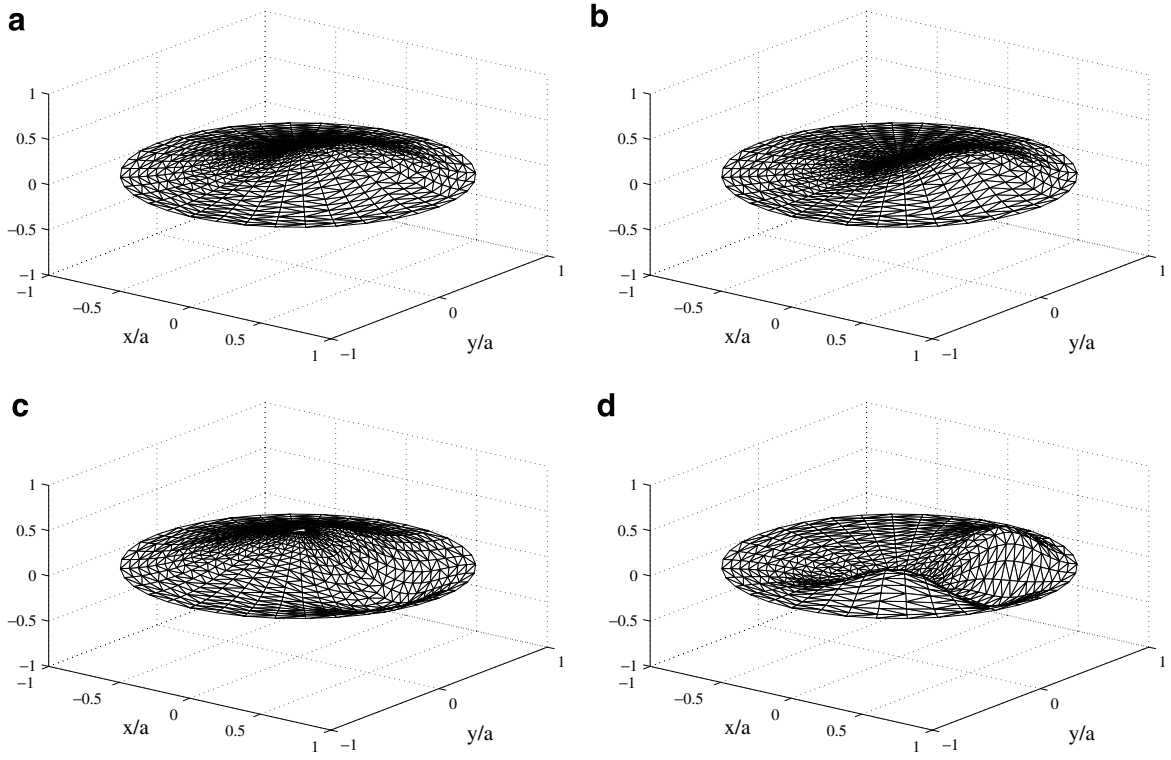

Fig. 4. Buckling of a radially compressed/stretched circular membrane in the presence of hydrodynamic load. First symmetric mode, S1, for $\nu = 0.45$ and (a) $\beta = -10$ ($\alpha = 38.27$), (b) $\beta = 10$ ($\alpha = 99.54$), (c) $\beta = -20$ ($\alpha = 66.74$), (d) $\beta = -28$ ($\alpha = 113.44$).

downstream portion of the membrane buckles due to compression, while the upstream part responds by developing a deflection to the downstream deformation.

A second symmetric solution branch in Fig. 3(a) originates from the critical point where the membrane buckles under the compressive pre-stress in the first Fourier mode, $n = 1$, in the absence of a hydrodynamic load, $\beta = -26.3746$ and $\alpha = 0$. The buckled shape for $\beta = -20$ corresponding to the critical load $\alpha = 66.74$ is shown in Fig. 4(c). This eigenfunction has a shape that is more convoluted than any of that described earlier

for the symmetric solution branch shown in Fig. 4(a and b). Further computations have revealed an infinite sequence of solution branches originating from the critical values of β in the absence of hydrodynamic load, listed in Table 1. As an example, Fig. 4(d) shows a buckled shape with two humps for $\beta = -28$ and $\alpha = 113.44$. The solution space of the first symmetric mode thus consists of a zig-saw pattern comprised of a sequence of segments originating from the zeros of Bessel functions.

The first antisymmetric mode described by the solid lines in Fig. 3(a) exhibits a similar behavior. The first solution branch in this case originates from the critical point $\beta = -26.3746$, $\alpha = 0$, where the membrane buckles under compression in the absence of hydrodynamic load. The critical value, α=136.33 for $\beta = 0$, is identical to that computed by Luo and Pozrikidis (2006) for an unstressed membrane. Buckled shapes for pre-compressed and pre-stretched membranes exhibiting notable oscillations are shown in Fig. 5(a–c). As in the case of the first symmetric mode, the solution space of the first antisymmetric mode consists of a zig-saw pattern consisting of a sequence of segments originating from the zeros of Bessel functions.

We have found that the critical point, $\beta = -26.3746$ and $\alpha = 0$, is a bifurcation point in the solution space, serving as a point of departure for symmetric and antisymmetric buckled modes. Since, when $\nu = 0.45$, the antisymmetric shape has a slightly lower threshold, α, it is most likely to be realized in practice. For a certain value of β, buckled shapes are possible at a sequence of values of α. For example, when $\beta = -14.6820$, a buckled shape occurs for $\alpha = 0$ corresponding to the axisymmetric deflection mode shown in Fig. 2(a). A second buckled shape occurs for $\alpha = 85.46$ corresponding to the antisymmetric mode shown in Fig. 6(a), and a third shape occurs for $\alpha = 89.95$ corresponding to symmetric mode shown in Fig. 6(b). Higher modes are shown in Fig. 6(c–f). The deformed shape shown in Fig. 6(b) is similar to that in Fig. 4(c), the shape shown in Fig. 6(c) is similar to that shown in Fig. 4(d), and the analogy persists for higher-order pairs.

Fig. 3(b) illustrates the solution space for the lower Poisson ratio, $\nu = 0.1$. The circles mark the critical conditions in the absence of pre-stretching occurring at α=81.3 for the symmetric mode, and at 169.20 for the

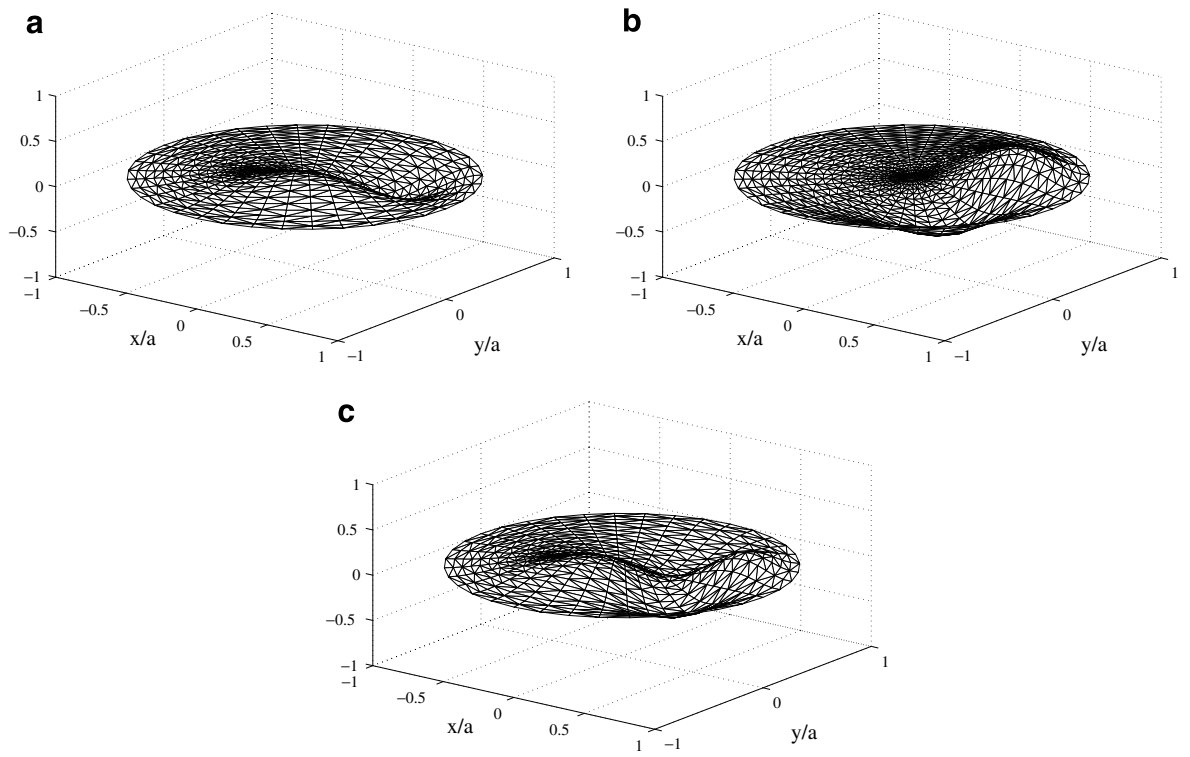

Fig. 5. Buckling of a radially compressed/stretched circular membrane in the presence of hydrodynamic load. First antisymmetric eigenmode, A1, for $\nu = 0.45$ and (a) $\beta = -20$ ($\alpha = 61.41$), (b) $\beta = 10$ ($\alpha = 165.52$), (c) $\beta = -28$ ($\alpha = 116.08$).

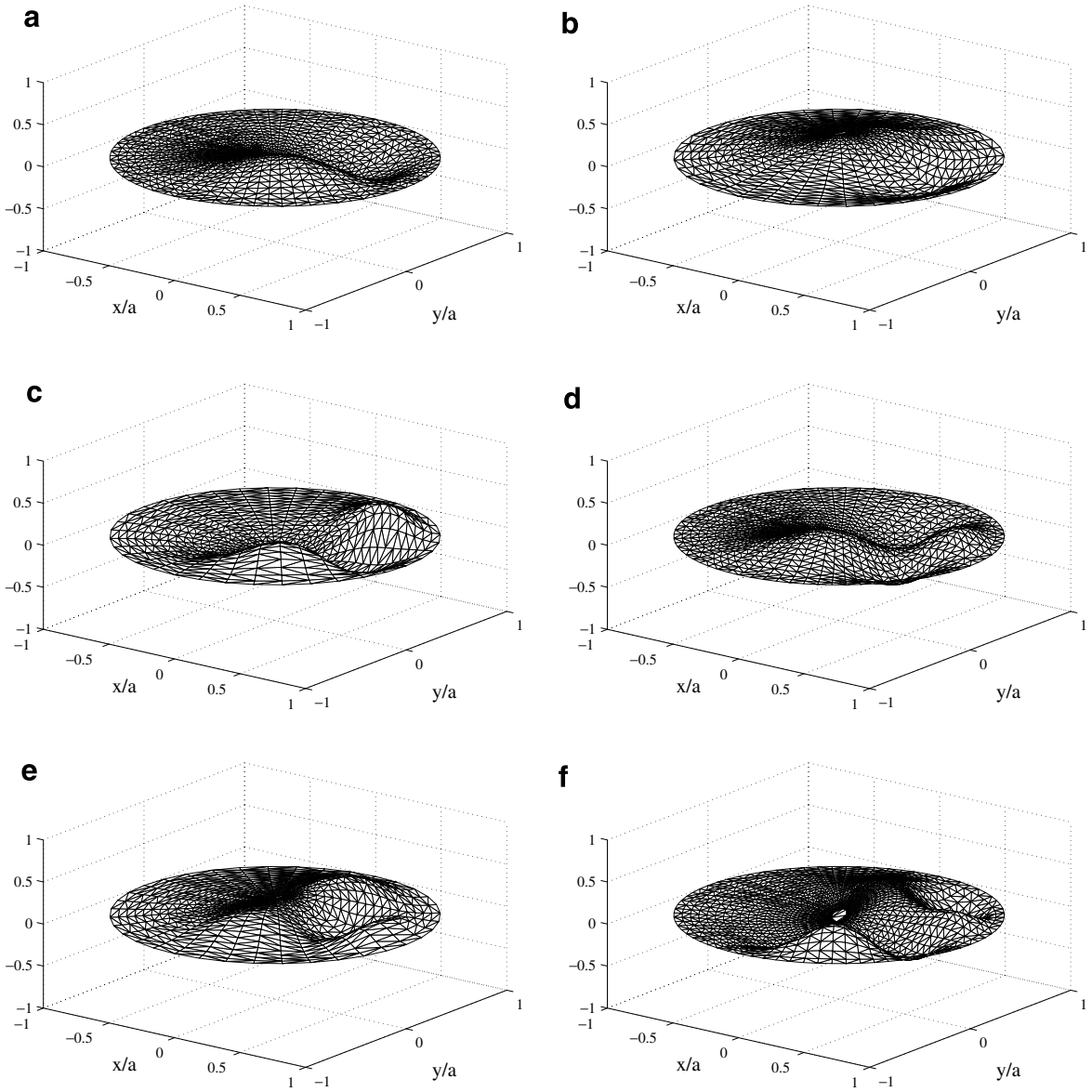

Fig. 6. Buckling eigenmodes for $\nu = 0.45$ and $\beta = -14.6820$: (a) $\alpha = 85.46$ (A1), (b) $\alpha = 89.95$ (S2), (c) $\alpha = 166.81$ (S3), (d) $\alpha = 168.54$ (A2), (e) $\alpha = 235.18$ (S4), and (f) $\alpha = 270.59$ (A3).

antisymmetric mode. The structure of the solution space and corresponding eigenfunctions are similar to those illustrated in the figures for $\nu = 0.45$. The symmetric and antisymmetric branches in Fig. 3(b) are separated by a wider margin than those shown in Fig. 3(a) for the higher Poisson ratio. The symmetric solution branches lie underneath the antisymmetric solution branches for the low Poisson ratio.

6. Discussion

We have computed critical solution branches in the (β, α) parametric space for the onset of buckling, and found that the flat membrane tolerates compression over a portion of its surface without buckling. The margin of tolerance was quantified by the difference between the critical value of α and the value where a local

compressive tension first occurs. Results presented in Fig. 3 reveal that this difference increases almost linearly at sufficiently high values of the pre-stress parameter β.

Each point on each branch is a bifurcation point of a certain solution plane described, for example, by the hydrodynamic shear stress, $\Delta\tau$, and curvature at the center of the circular patch. In the linearized analysis presently undertaken, only shapes near the bifurcation points were described to first order with respect to the membrane deflection amplitude. To describe substantially deformed shapes, a non-linear postbuckling analysis based on the full von Kármán equation must be pursued using numerical method (e.g., Dossou and Pierre, 2003).

When a membrane buckles in a fluid, the deformation of the evolving shape is resisted by hydrodynamic viscous stresses of the induced perturbation flow riding on the simple shear flow. The time scale of the evolution is thus determined by the fluid viscosities and length scale of the developing corrugations. For the corrugations to amplify and become visible, the duration of compression must be sufficiently long. If a membrane patch on the capsule undergoes periodic compression and extension, permanent wrinkling will arise only under favorable conditions. An integrated analysis of the pertinent dynamics will be undertaken in future work.

Acknowledgment

Support for this research was provided by the National Science Foundation.

References

Bloom, F., Coffin, D., 2001. Handbook of Thin Plate Buckling and Postbuckling. Chapman & Hall, Boca Raton.

Boal, H., Seifert, U., Shillock, J.C., 1993. Negative Poisson ratio in two-dimensional networks under tension. l l E 48, 4274–4283.

Dossou, K., Pierre, R., 2003. A Newton-GMRES approach for the analysis of the postbuckling behavior of the solutions of the von Kármán equations. SIAM Journal of Scientific Computing 24, 1994–2012.

Fung, Y.C., 1965. Foundations of Solid Mechanics. Prentice-Hall, Englewood Cliffs.

Lac, E., Barthés-Biesel, D., 2005. Deformation of a capsule in simple shear flow: effect of membrane prestress. Physics of Fluids 17, 072105.

Luo, H., Pozrikidis, C., 2006. Buckling of a flush-mounted plate in simple shear flow. Archives of Applied Mechanics 76, 549–566.

Pieper, G., Rehage, H., Barthès-Biesel, D., 1988. Deformation of a capsule in a spinning drop apparatus. Journal of Colloid and Interface Science 202, 293–300.

Schmid-Schoenbein, G.W., Kosawada, T., Skalak, R., Chien, S., 1995. Membrane model of endothelial-cells and leukocytes – a proposal for the origin of a cortical stress. Journal of Biomechanical Engineering ASME 117, 171–178.

Timoshenko, S.P., Gere, J.M., 1961. Theory of Elastic Stability, Second ed. McGraw Hill, New York.

Walter, A., Rehage, H., Leonhard, H., 2001. Shear-induced deformations of microcapsules: shape oscillations and membrane folding. Colloids and Surfaces A, Physicochemical and Engineering Aspects 183, 123–132.

Wang, C.Y., 2005. On the buckling of a circular plate on an elastic foundation. Journal of Applied Mechanics 72, 795–796.